J|A|C|S
ARTICLES
Published on Web 02/18/2006

Synthesis, Structure, and Magnetic Properties of Li-Doped Manganese-Phthalocyanine, Li_x[MnPc] ($0 \leqslant x \leqslant 4$)

Yasujiro Taguchi,*[,†,‡] Toshiaki Miyake,[†] Serena Margadonna,*[,§] Kenichi Kato,[‡,||] Kosmas Prassides,*[,⊥] and Yoshihiro Iwasa[†,‡]

Contribution from the Institute for Materials Research, Tohoku University, Sendai 980-8577, Japan, CREST, Japan Science and Technology Corporation, Kawaguchi 332-0012, Japan, the School of Chemistry, University of Edinburgh, Edinburgh EH9 3JJ, U.K., JASRI/SPring-8, 1-1-1 Kouto, Sayo-cho, Sayo-gun, Hyogo 679-5198, Japan, and the Department of Chemistry, University of Durham, Durham DH1 3LE, U.K.

Received December 21, 2005; E-mail: taguchi@imr.tohoku.ac.jp; serena.margadonna@ed.ac.uk; K.Prassides@dur.ac.uk

Abstract: We report on the first synthesis of Li-intercalated manganese-phthalocyanine (MnPc) in the bulk form and on the evolution of the structural and magnetic properties as a function of Li concentration, *x*. We find that solid β-MnPc, which comprises rodlike assemblies of individual planar molecules, is best described as a glassy one-dimensional ferromagnet without three-dimensional ordering and that it can be quasi-continuously intercalated with Li up to $x = 4$, forming an isosymmetrical series of Li_x[MnPc] phases. Inserted Li^+ ions strongly bond to pyrrole-bridging nitrogen atoms of the Pc rings, thereby disrupting the ferromagnetic $Mn-N_a\cdots Mn$ superexchange pathways. This gradually induces a crossover of the intrachain exchange interactions from ferromagnetic to antiferromagnetic as the doping level, *x*, increases coupled with a spin-state transition of the Mn^{2+} ions from intermediate spin, $S = 3/2$, to high spin, $S = 5/2$.

Introduction

The metal phthalocyanine molecules (denoted as MPc, hereafter) comprise a very stable π-conjugated macrocyclic ligand that incorporates a metal ion in the void at the center of the molecule. They form a diverse class of multifunctional materials, which display interesting and useful optical, electronic, catalytic, and biological properties.[1] Planar MPc molecules invariably crystallize in the solid state as weakly coupled one-dimensional stacks, forming "herringbone structures", and therefore, their various physical properties, such as conductivity, magnetism, and optical response, are strongly anisotropic. Two polymorphic (α- and β-) MPc forms are frequently encountered in the solid state.[2,3] These differ in both the intrastack packing architecture and the relative interchain orientations. The tilting angle, defined as the angle between the stacking direction and the normal to the plane of each molecule, is about 27° and 45° for the α- and β-forms, respectively. The difference in stacking is reflected in the overlap of the wave functions between π-electrons belonging to adjacent molecules being larger in the α- than in the β-form of MPc. It is empirically known that MPc crystalline solids adopt the β-form in the bulk, whereas the α-form is frequently encountered in thin films. The α-polymorphs easily transform to the β- form on heating above about 300 °C.

A characteristic feature of MPc solids is that the divalent metal ion at the center of the macrocycle can bear a magnetic moment, and thus, MPc systems show intriguing magnetic properties, including ferromagnetic-like behavior. One such example is provided by the β-polymorph of MnPc, in which Mn^{2+} is in the unusual intermediate spin state with $S = 3/2$ and possesses Ising-like anisotropy along the direction perpendicular to the molecule. The neighboring spins are coupled ferromagnetically along the chain direction, and this material exhibits a steep rise of the magnetic moment in a magnetic field as well as a hysteresis loop at low temperatures that are characteristic of ferromagnets.[4−7] These observations have been regarded as evidence for a ferromagnetic transition at low temperatures below about 9 K, and β-MnPc has been referred to as a typical example of a molecular magnet.[8] However, as we will show in the present paper, the spins in β-MnPc are ordered only along the chain direction while they remain three-dimensionally disordered. A similar ferromagnetic-like behavior at low temperatures was also recently reported for the α-form of FePc with the magnetization beginning to increase rapidly at about 15 K in a low field and the *MH* curve at 1.8 K showing

[†] Tohoku University.
[‡] CREST.
[§] University of Edinburgh.
[||] JASRI/Spring-8.
[⊥] University of Durham.

(1) McKeon, N. B. *Phthalocyanine Materials*; Cambridge University Press: Cambridge, 1998.
(2) Figgis, B. N.; Kucharski, E. S.; Williams, G. A. *Dalton Trans.* **1980**, 1515−1525. Figgis, B. N.; Mason, R.; Williams, G. A. *Acta Crystallogr., Sect. B* **1980**, *36*, 2963−2970.
(3) Hoshino, A.; Takenaka, Y.; Miyaji, H. *Acta Crystallogr., Sect. B* **2003**, *59*, 393−403.
(4) Barraclough, C. G.; Martin, R. L.; Mitra, S.; Mitra, S. *J. Chem. Phys.* **1970**, *53*, 1638−1642.
(5) Miyoshi, H.; Ohya-Nishiguchi, H.; Deguchi, Y. *Bull. Chem. Soc. Jpn.* **1973**, *46*, 2724−2728.
(6) Mitra, S.; Gregson, A. K.; Hatfield, W. E.; Weller, R. R. *Inorg. Chem.* **1983**, *22*, 1729−1732.
(7) Awaga, K.; Maruyama, Y. *Phys. Rev. B* **1991**, *44*, 2589−2594.
(8) Kahn, O. *Molecular Magnetism*; VCH Publishers: New York, 1993; p 323.

a clear hysteresis.[9] However, the ac susceptibilities at low temperature were frequency dependent implying the relevance of slow relaxation processes. On the basis of these characteristic features, it was concluded that the ground state of α-FePc is composed of very weakly coupled ferromagnetic segments that remain disordered even at the lowest temperature reached. This kind of magnetic state could be relevant to the emerging field of the so-called "single-chain magnets".[10−12] In these materials, a tunneling gap is formed between the up and down spin states due to the Ising anisotropy of the ferromagnetically coupled one-dimensional (1D) spin system with the spin dynamics explained in terms of Glauber's theory for 1D magnets.[13] Alternatively, a spin glass state may also be responsible for the slow relaxation process observed. In this case, the gap is established by the multivalley structure of the free energy arising from magnetic frustration or disorder effects.

Electric conduction of MPc systems thus far has been only achieved[14,15] by introducing holes through reactions with electron acceptors because of the good electron-donating ability of MPc molecules. Hole doping into MPc was first demonstrated successfully[16] by means of iodination of NiPc to afford the highly conducting molecular solid $NiPc(I_3)_{0.33}$. Since then, many families of molecular metals employing hole-doped cofacially stacked MPc units as building blocks have been synthesized and characterized.[17−20] Among these studies, polarized reflectance measurements[17] on single-crystal samples of $NiPc(SbF_6)_{0.5}$ and $NiPc(AsF_6)_{0.5}$ have clearly demonstrated the one-dimensionality of the metallic state that has been achieved by the hole doping. In $Cu_x(H_2)_{1-x}PcI$, interplay between the localized magnetic moments of Cu^{2+} and the charge carriers was also observed.[18−20] Even more dramatic phenomena of gigantic negative magnetoresistance effects have been reported[21] for $TPP[FePc(CN)_2]_2$ (TPP = tetraphenylphosphonium), stimulating extensive recent theoretical work.[22]

In contrast to the extensive hole-doping chemistry, the synthesis of electron-doped MPc assemblies has remained virtually unexplored. However, metallic conduction has recently been reported in alkali-metal-doped MPc thin films,[23] thereby providing novel opportunities in MPc research of electron doping of MPc systems. Stimulated by these experimental studies, Tosatti et al. have theoretically investigated the electronic phase diagram of electron-doped MPc solids.[24] In particular, electron doping into the 2-fold degenerate lowest unoccupied molecular orbital of MPc is expected to lead to strongly correlated electron systems (doped two-band Mott insulators)[24] displaying a rich electronic phenomenology akin to electron-doped fullerides. The resulting physics is predicted to be much richer than that of their hole-doped counterparts, in which electron transfer involves a nondegenerate highest occupied molecular orbital, because of the expected strong electron−phonon interaction that lifts the double degeneracy of the lowest unoccupied molecular orbital. However, given at present the lack of any isolated and structurally characterized alkali-doped MPc material, the whole theoretical picture rests on the assumption that there is little structural renormalization of the MPc lattice upon alkali doping with the dopants exclusively residing in the interstack spacing. To make any progress in this research area of electron doping of the vast family of metallophthalocyanines, it is imperative to successfully synthesize single-phase samples of alkali-metal intercalated MPc in the bulk, to fully identify the structures adopted and to explore the electronic and physical properties such as magnetism and conduction.

In this article, we report on the first synthesis of a series of crystalline Li-doped β-MnPc phases and on the evolution of their structural and magnetic properties as a function of Li concentration. We have found that there exists an isosymmetrical series of $Li_x[MnPc]$ phases where Li is quasi-continuously intercalated up to $x = 4$. Depending on the doping level, Li insertion is accompanied by changes in the intrastack and interstack packing motifs and is found to gradually induce a crossover of the intrachain exchange interactions from ferromagnetic to antiferromagnetic coupled with a spin-state transition of the Mn^{2+} ions from intermediate spin, $S = 3/2$, to high spin, $S = 5/2$.

Experimental Details

As-purchased MnPc powder was purified by multiple vacuum sublimation at 450−500 °C. All physical measurements on undoped MnPc were performed on triply sublimed samples. Li intercalation to afford samples with stoichiometry $Li_x[MnPc]$ was carried out using a liquid-phase reaction protocol in an Ar-filled glovebox using stoichiometric amounts of *n*-butyllithium and MnPc. Singly sublimed MnPc powders (ca. 30 mg) were dispersed in *n*-BuLi/hexane solutions (ca. 3 mL) of the appropriate molarity for the intended doping value x ($0 < x \leq 4$) for 1 day. All solutions used were obtained by dilution of a 1.6 M *n*-BuLi/hexane solution. In addition, we also used the undiluted solution to prepare samples doped to saturation. The powders were collected by filtration and were subjected to annealing procedures in a vacuum at 200−300 °C for 2 days. Phase purity was confirmed by laboratory powder X-ray diffraction. Li concentrations in the products were determined by the inductively coupled plasma spectroscopy (ICP) technique.

High-resolution synchrotron X-ray diffraction measurements were performed on powdered samples sealed in 0.5-mm diameter glass capillaries. Synchrotron X-ray powder diffraction patterns were recorded at ambient temperature with the high-resolution powder diffractometers on beamline BL02B2 ($\lambda = 1.0007$ Å, $2\theta = 2°-40°$) at SPring-8, Japan, and on beamline ID31 ($\lambda = 0.85045$ Å, $2\theta = 2°-30°$) at the European Synchrotron Radiation Facility (ESRF), Grenoble, France. Data analysis was performed with the GSAS suite of Rietveld analysis programs.

(9) Evangelisti, M.; Bartolome, J.; de Jongh, L. J.; Filoti, G. *Phys. Rev. B* **2002**, *66*, 144410.
(10) Caneschi, A.; Gatteschi, D.; Lalioti, N.; Sangregorio, C.; Sessoli, R.; Venturi, G.; Vindigni, A.; Rettori, A.; Pini, M. G.; Novak, M. A. *Angew. Chem.* **2001**, *40*, 1760−1763.
(11) Clerac, R.; Miyasaka, H.; Yamashita, M.; Coulon, C. *J. Am. Chem. Soc.* **2002**, *124*, 12837−12844.
(12) Miyasaka, H.; Clerac, R.; Mizushima, K.; Sugiura, K.; Yamashita, M.; Wernsdorfer, W.; Coulon, C. *Inorg. Chem.* **2003**, *42*, 8203−8213.
(13) Glauber, R. J. *J. Math. Phys.* **1963**, 4, 294−307.
(14) Marks, T. J. *Angew. Chem.* **1990**, *29*, 857−879.
(15) Inabe, T.; Tajima, H. *Chem. Rev.* **2004**, *104*, 5503−5533.
(16) Schramm, C. J.; Scaringe, R. P.; Stojakovic, D. R.; Hoffman, B. M.; Ibers, J. A.; Marks, T. J. *J. Am. Chem. Soc.* **1980**, *102*, 6702−6713.
(17) Yakushi, K.; Yamakado, H.; Yoshitake, M.; Kosugi, N.; Kuroda, H.; Sugano, T.; Kinoshita, M.; Kawamoto, A.; Tanaka, J. *Bull. Chem. Soc. Jpn.* **1989**, *62*, 687−696.
(18) Ogawa, M. Y.; Hoffman, B. M.; Lee, S.; Yudkowsky, M.; Halperin, W. P. *Phys. Rev. Lett.* **1986**, *57*, 1177−1180.
(19) Thompson, J. A.; Murata, K.; Durcharne, R.; Poirier, M.; Hoffman, B. M. *Phys. Rev. B* **1999**, *60*, 523−529.
(20) Martin, I.; Phillips, P. *Phys. Rev. B* **1999**, *60*, 530−532.
(21) Hanasaki, N.; Tajima, H.; Matsuda, M.; Naito, T.; Inabe, T. *Phys. Rev. B* **2000**, *62*, 5839−5842.
(22) Hotta, C.; Ogata, M.; Fukuyama, H. *Phys. Rev. Lett.* **2005**, *95*, 216402.
(23) Craciun, M. F.; Rogge, S.; den Boer, M. J. L.; Margadonna, S.; Prassides, K.; Iwasa, Y.; Morpurgo, A. F. *Adv. Mater.* **2006**, *18*, 320−324. Craciun, M. F.; Rogge, S.; Morpurgo, A. F. *J. Am. Chem. Soc.* **2005**, *127*, 12210−12211.
(24) Tosatti, E.; Fabrizio, M.; Tobik, J.; Santoro, G. E. *Phys. Rev. Lett.* **2004**, *93*, 117002.

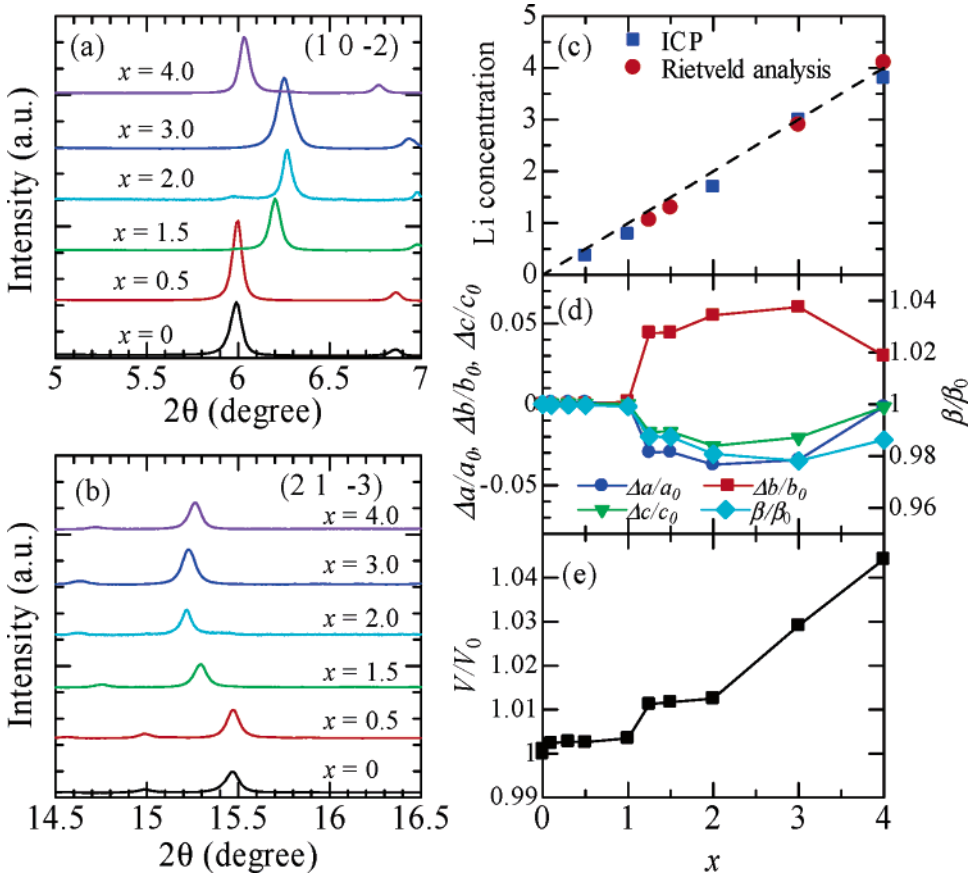

Figure 1. (a) and (b) Selected regions of the ambient-temperature synchrotron X-ray (λ = 1.0007 Å) diffraction profiles of Li_x[MnPc] (x = 0, 0.5, 1.5, 2, 3, and 4) showing the evolution of the $(10\bar{2})$ and $(21\bar{3})$ Bragg reflections with x. (c) Correlation between nominal Li concentration, x, and those obtained from inductively coupled plasma spectroscopy (ICP) analysis (blue squares) and Rietveld analysis of the X-ray diffraction data (red circles). (d) and (e) Evolution of the change in the monoclinic lattice constants, a, b, c, and β, and the normalized unit cell volume, V/V_0, in Li_x[MnPc] with Li concentration, x.

Low- (30 Oe) and high-field (2 kOe) dc magnetization measurements were performed between 2 and 300 K on samples sealed in quartz tubes using a Quantum Design SQUID magnetometer (equipped with an ac option). The background contributions from the quartz tubes were then subtracted. Ac susceptibilities were measured in zero applied static field with an oscillating field (3 Oe) at various frequencies in the range 1−1500 Hz. The resistivity of selected Li_x[MnPc] pellets was also measured inside the glovebox by the two-probe method; the electrical contacts were made with silver paste. We also recorded the resistivity of one of the samples by the four-probe method and confirmed that the resistivity values deduced from the two techniques were compatible to each other. We finally measured the temperature dependence of the heat capacity (Physical Property Measurement System, Quantum Design) of pristine triply sublimed MnPc and NiPc samples pressed into pellets together with Ag powder to facilitate thermal equilibration. The Ag contribution to the heat capacity was measured in a separate run and subtracted from the data.

Results

Chemical Analysis. The Li concentrations in the Li_x[MnPc] samples determined by the ICP technique are plotted in Figure 1c as a function of the nominal Li content, x. The excellent agreement between the measured and nominal doping values confirms that all Li from the reactant *n*-BuLi solutions is essentially intercalated in the course of the reactions into the MnPc host lattice. For the Li_x[MnPc] samples prepared from undiluted *n*-BuLi solutions, the ICP analysis shows a Li concentration of about 4, implying that the saturation composition of these phases has the stoichiometry Li_4[MnPc].

Structural Evolution upon Li Intercalation. The Li_x[MnPc] phase diagram was first surveyed as a function of Li content with x varying between 0 and 4. Inspection of the ambient-temperature high-resolution synchrotron X-ray diffraction profiles of the powder samples (Figure 1a,b) readily revealed remarkable similarities with that of pristine β-MnPc implying that these materials were single phase and formed an isosymmetric structural series. All reflections index on the primitive monoclinic (space group $P2_1/c$) unit cell of the pristine β-MnPc phase,[2] and the crystal structure remains strictly unchanged throughout the compositional range. However, the angular positions of the diffraction peaks shift systematically as the Li doping level x varies, implying that the unit cell metrics sensitively depend on the magnitude of x. LeBail refinements of the diffraction data were thus first employed to extract accurate values of the lattice parameters. Figures 1d and 1e show the evolution of the extracted lattice constants and the unit cell volume with increasing doping level, respectively. The unit cell volume first increases marginally up to $x \sim 1$ but then continuously and rapidly inflates, eventually approaching an overall increase of 4.5% for $x \sim 4$. This provides an unambiguous signature of Li intercalation into empty spaces of the structure of pristine β-MnPc without significantly perturbing the basic stacking architecture. However, the individual monoclinic lattice constants, a, b, and c, do not respond in the same way, as the Li doping level increases above 1 and the short axis b, which defines the slipped stacking direction of the MnPc

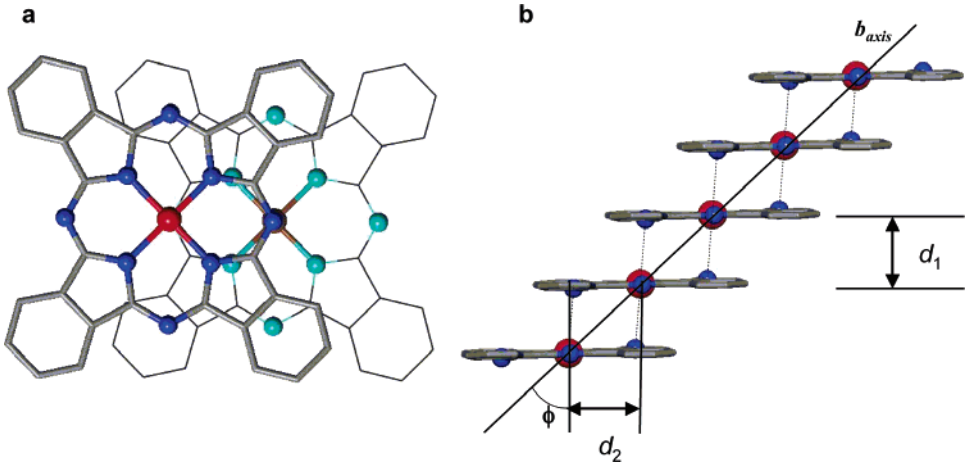

Figure 2. (a) Projection of two neighboring MnPc molecules within the same stack along the normal direction to their planar rings in β-MnPc. The Mn^{2+} ions are depicted as red (brown) spheres lying directly above (below) neighboring light blue (dark blue) N atoms. (b) The slip-stacked MnPc assemblies along the *b* axis that make up the monoclinic (space group $P2_1/c$) crystal structure of β-MnPc. The $Mn-N_a\cdots Mn$ units which define the one-dimensional ferromagnetic exchange pathways along *b* are emphasized by dotted blue lines. d_1 (3.16 Å), d_2 (3.55 Å), and ϕ (48.2°) mark the intrastack distance, the slipping distance, and the slipping angle, respectively, for β-MnPc.

columns, sharply increases for $x > 1$; the lattice constants *a* and *c*, which reflect the interchain separations, sharply decrease. This trend survives up to $x \sim 3$, but it is finally reversed for the Li_4[MnPc] composition when *b* contracts and *a* and *c* expand.

To address the nonmonotonic structural response of MnPc to Li intercalation, we proceeded with an accurate analysis of the synchrotron X-ray powder diffraction data across the Li_x[MnPc] series by employing conventional Rietveld refinements, combined with simulated annealing and difference Fourier map techniques. As there are no examples known in the literature of any other alkali-metal intercalated MPc systems, the search for the location of the intercalated Li^+ is a formidable task, especially given the weak X-ray scattering power of this light element. The β-polymorph of MnPc adopts a monoclinic structure ($a = 14.764$ Å, $b = 4.764$ Å, $c = 19.422$ Å, and $\beta = 120.70°$; space group $P2_1/c$) in which the planar metallomacrocycles form slip-stacked 1D columns along the short *b* axis with an interplanar separation, d_1, of 3.16 Å (Figure 2).[2] The slipped packing motif of MnPc molecules is such that two pyrrole-bridging N_a atoms of each Pc unit lie at 3.16 Å almost directly above or below the Mn(II) ions of its two nearest neighbors ($Mn-N_a\cdots Mn = 93.4°$). Adjacent stacks are inclined by symmetry at an angle of 90° and are well separated from each other at a distance of 10.00 Å.

We first describe our Rietveld analysis results for the Li_x[MnPc] ($x = 1.25$, 1.5) phases. As there is excellent correspondence of the reflection positions in the ambient-temperature diffraction profiles of the Li_x[MnPc] phases with those observed in β-MnPc, the Rietveld refinements were initiated in the monoclinic space group $P2_1/c$ with the starting structural model based on that of β-MnPc. Difference Fourier analysis of both $x = 1.25$ and $x = 1.5$ diffraction datasets revealed the existence of scattered intensity in the vicinity of the 4*e* (0.09, −0.18, 0.88) sites of the unit cell. These are located in the intracolumnar spacing between successively stacked MnPc units. Thus, the subsequent simulated annealing optimization of the geometry of the MnPc moieties and the conventional Rietveld refinements were undertaken after introducing a Li^+ ion in these 4*e* sites and allowing for its position and occupation number to vary. The latter converged to 1.06(2) and 1.30(4) per MnPc unit, respectively, in excellent accord with the expected composition of the two phases and implying that the intercalated Li^+ is disordered over two intrachain interstices. The results of the final refinement for $Li_{1.25}$[MnPc] are shown in Figure 3a (lattice constants: $a = 14.3639(2)$ Å, $b = 4.9768(1)$ Å, $c = 18.8322(3)$ Å, $\beta = 119.229(2)°$; agreement factors: $R_{wp} = 3.14\%$, $R_{exp} = 4.06\%$) with fitted parameters listed in Table 1 and in Supporting Information Table 1S. Although it did not prove possible to locate the Li^+ defect in the lightly doped Li_x[MnPc] ($x \leq 0.5$) phases given its weak contribution to the overall scattered intensity, it is reasonable to assume from the general evolution of the lattice metrics discussed before (Figure 1d) that it also partially occupies the same sites as when $x > 1$.

The results of these structural refinements show that the response of the 1D MnPc packing architecture to the Li^+ insertion is very different from that ubiquitously encountered in hole-doped MPc phases following intercalation with electron acceptors when the packing architecture of the pristine material changes in such a way that the MPc units form nonslipped staggered stacks with chains of counteranions, such as I_3^-, extending parallel to the stacking direction.[14,15] In the Li_x[MnPc] family, despite the increased value of the *b* lattice constant by 4.5% at $x \sim 1.5$, the building structural motif of the chains and the intrastack separation change very little. Instead, the MnPc units allow for the accommodation of the Li^+ ions by increasing their slipping distance relative to each other along the stacking direction. This results progressively in an increased intermolecular $Mn\cdots N_a$ distance to ~3.21 Å and an opening up of the $Mn-N_a\cdots Mn$ angle to ~98°. Very importantly, the refined intercalated Li^+ position within the stacks is also physically meaningful, and the occupied interstitial sites are such that every Li^+ lies at ~2.0 Å directly above (or below) the very same pyrrole-bridging N_a atoms of the Pc units that also coordinate to Mn(II) ions of neighboring MnPc molecules (Figure 4). The increased slippage of the stacks is crucial in removing steric hindrance between the Li^+ ions and near neighboring units along the stacking direction, and at the same time, the lack of off-

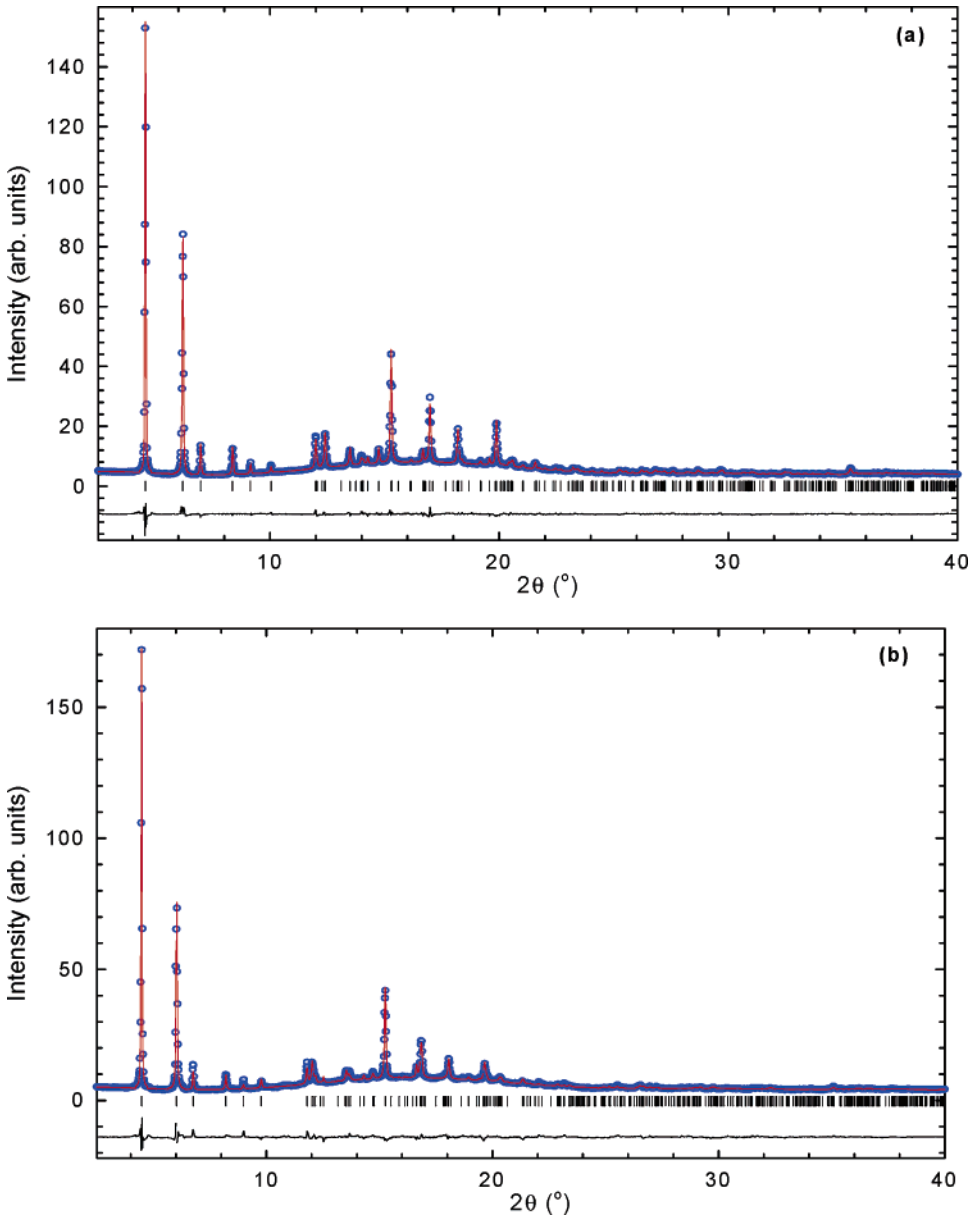

Figure 3. Final observed (○) and calculated (solid line) powder synchrotron X-ray ($\lambda = 1.0007$ Å) diffraction profiles for (a) $Li_{1.25}$[MnPc] and (b) Li_4-[MnPc] at ambient temperature. In each case, the lower solid line shows the difference profile and the tick marks show the reflection positions.

Table 1. Refined Li Positions and Fractional Occupancies, *n*, in the Li_x[MnPc] Series[a]

nominal *x*		*x*/*a*	*y*/*b*	*z*/*c*	*n*	refined *x*
1.25	Li(1)	0.093(1)	−0.188(5)	0.877(1)	0.53(1)	1.06(2)
1.5	Li(1)	0.091(2)	−0.177(6)	0.879(2)	0.64(2)	1.30(4)
3	Li(1)	0.075(6)	−0.166(4)	0.872(4)	0.60(3)	2.98(6)
	Li(2)	0.327(4)	0.817(4)	0.319(4)	0.89(3)	
4	Li(1)	0.098(5)	−0.106(7)	0.898(2)	0.84(3)	4.10(6)
	Li(2)	0.307(5)	0.840(6)	0.263(2)	0.71(3)	
	Li(3)	0.5	0	0	1.0	

[a] ($x = 1.25$, 1.5, 3, and 4)[25].

axis counterions leads to a contraction (to 9.74 Å at $x \sim 1.5$) of the separation of adjacent MnPc chains.

The unit cell metrics in the Li_x[MnPc] family continue to evolve monotonically on further doping with Li up to $x \sim 3$ with the short *b* axis increasing to 5.072 Å and the *a* and *c* axes contracting further (Figure 1d). However, the intrastack holes in which the Li^+ ions reside at low-to-moderate doping levels should become filled at $x = 2$. This implies that further Li doping must lead to the occupation of additional interstitial sites in the unit cell. Rietveld refinement of the diffraction data of the isostructural Li_3[MnPc] composition was attempted following a systematic search of additional interstitial sites in the unit cell. Stable refinements were achieved when dopants were also introduced into 4*e* (0.68, 0.22, 0.27) intrachain sites of the unit cell. The refined doping level, *x*, converged to 2.98-(6) per MnPc unit in good agreement with the expected stoichiometry (lattice constants: $a = 14.3094(6)$ Å, $b = 5.0522$-(3) Å, $c = 18.7354(7)$ Å, $\beta = 118.073(4)°$; agreement factors: $R_{wp} = 4.87\%$, $R_{exp} = 3.53\%$). The new Li^+ geometry is such that there is strong coordination at ~2.0 Å to one of the other pyrrole-bridging N_b atoms (at 90° to the N_a atoms) of the Pc macrocycles. The Li^+ defects are now almost uniformly disordered over the corners of a (Li_4) rectangle residing in the space defined by adjacent MnPc units in the same chain (Figure 5a). A notable feature of the crystal structure at this composition

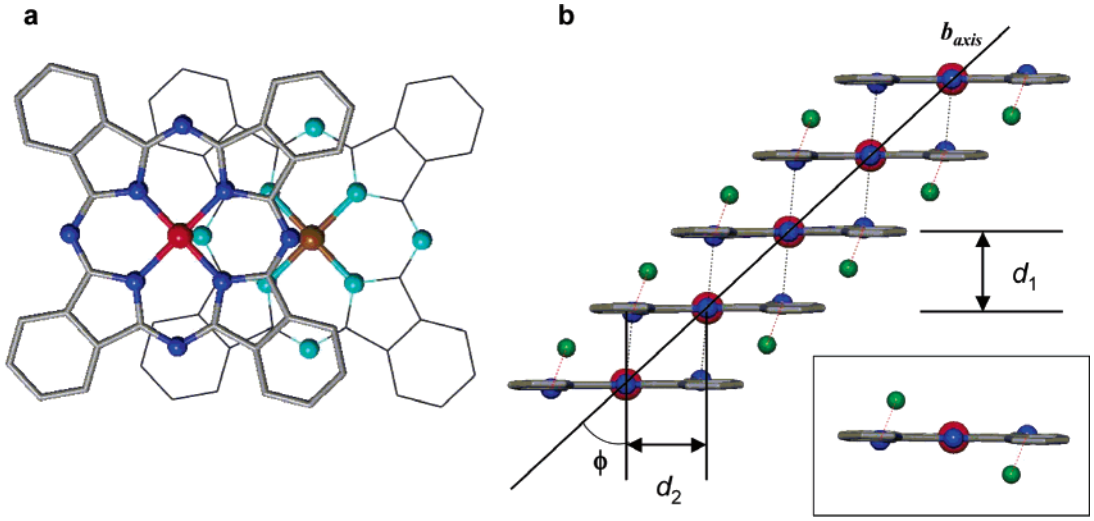

Figure 4. (a) Projection of two neighboring MnPc molecules within the same stack along the normal direction to their planar rings in $Li_{1.5}$[MnPc], emphasizing their increased relative slippage when compared to the pristine material. Labeling is as in Figure 2. (b) The slip-stacked MnPc assembly along the *b* axis in $Li_{1.5}$[MnPc] ($d_1 = 3.18$ Å, $d_2 = 3.84$ Å, $\phi = 50.3°$). Li^+ ions (Li(1), depicted in green) are disordered and reside exclusively in the intrastack spacing and bond strongly to pyrrole-bridging N atoms (red dotted lines). The inset shows the Li_2MnPc building block of the 1D assemblies.

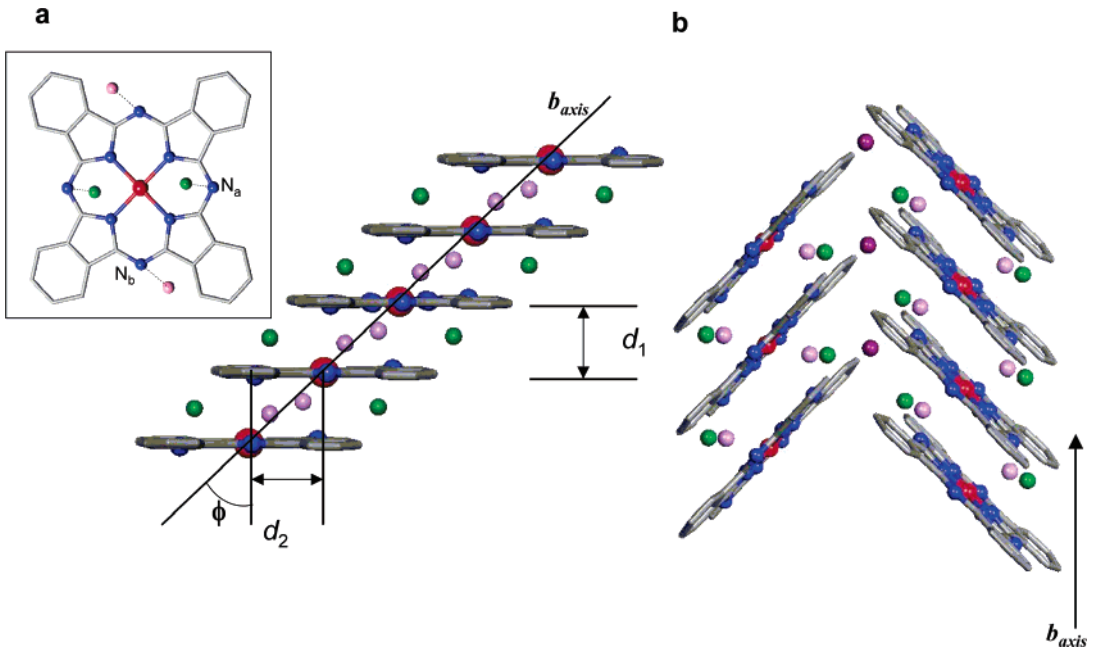

Figure 5. (a) Slip-stacked MnPc assembly along the *b* axis in Li_3[MnPc] ($d_1 = 3.25$ Å, $d_2 = 3.87$ Å, $\phi = 50.0°$). Disordered Li^+ ions (depicted in green and pink) again reside exclusively in the intrastack spacing. The inset shows the Li_4[MnPc] building block of the 1D assemblies. (b) Projection of two adjacent chains inclined at 90° and running along the *b* axis in Li_4[MnPc]. In addition to Li^+ ions (Li(1), green, and Li(2), pink spheres) accommodated in the intrastack spacing as before, additional Li^+ ions (Li(3), violet spheres) also occupy interstack interstices.

is that the extra Li doping leads to an increase in the intrastack separation and therefore in the intermolecular Mn···N_α distance to ~3.29 Å, whereas both the relative slipping of the MnPc units with respect to each other and the Mn−N_α···Mn angle remain essentially unchanged. As no Li^+ is accommodated in the spacing between adjacent chains, their distance continues to contract further to 9.70 Å.

Finally, saturation doping of MnPc affords the Li_4[MnPc] phase whose diffraction profile evidences a strong renormalization of the unit cell constants, despite retaining the same monoclinic crystal structure. The most notable feature of this end composition is that the trend in the gradual shortening of the separation of adjacent chains with increasing Li content is suddenly reversed. The extracted value is 9.99 Å, comparable to that in pristine β-MnPc. This provides the signature that Li is now also accommodated at interstitial holes between the stacks (Figure 5b). Its position was identified in the course of the Rietveld refinements as the high-symmetry 2*b* (1/2, 0, 0) site, which presents no sterical crowding and is fully occupied. The results of the final Rietveld refinement for Li_4[MnPc] are shown in Figure 3b ($a = 14.6011(7)$ Å, $b = 4.9086(2)$ Å, $c = 19.3846(7)$ Å, and $\beta = 119.063(5)°$; agreement factors: $R_{wp} = 4.81\%$, $R_{exp} = 3.99\%$) with fitted structural parameters listed in Table 1 and in Supporting Information Table 2S. The refined Li doping level converged to 4.10(6) per MnPc unit.[25] We note that the

(25) The fractional occupancy, *n*, of the Li(3) atom in Li_4[MnPc] was originally allowed to vary, converging to a value slightly larger than 1. In the final stages of the Rietveld refinements, *n* was fixed to 1.

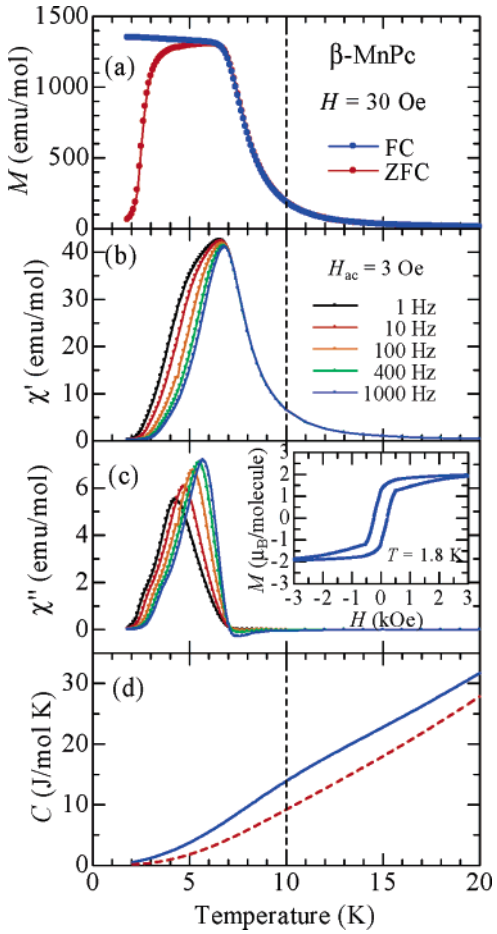

Figure 6. Temperature dependence of (a) the dc magnetization, M, at H = 30 Oe in field-cooling (FC) and zero-field-cooled-warming (ZFC) runs, (b) the real part of the ac susceptibility, χ', (c) the imaginary part of the ac susceptibility, χ'', and (d) the heat capacity, C, of pristine β-MnPc (blue solid curve) and the estimated lattice contribution from complementary measurements on β-NiPc (red dashed curve). See text for the way to estimate the lattice contribution. The inset of panel (c) shows the isothermal MH curves at 1.8 K. The dashed line at 10 K indicates the temperature (T*) where dc magnetization begins to increase rapidly.

refined Li^+ content is in excellent agreement with both the nominal concentration and that derived from chemical analysis for all Li_x[MnPc] compositions studied, as shown in Figure 1c.

Resistivity Measurements. We have also measured the resistivity of the Li-doped polycrystalline samples by the conventional two-probe method at room temperature. The values (Supporting Information Figure 1S) remained high (=400 kΩ cm − 20 MΩ cm) throughout the doping range of $0 \leq x \leq 4$, and the measured resistivity did not show any considerable decrease from that of pristine MnPc (8 MΩ cm).

Magnetic Properties. Figure 6a shows the temperature variation of the magnetization of triply sublimed pristine β-MnPc in a low magnetic field (30 Oe) both in field-cooling (FC) and in zero-field-cooled-warming (ZFC) runs. The magnetization begins to increase rapidly at about 10 K with decreasing temperature for both FC and ZFC protocols. This magnetic response together with the observed hysteresis at T = 1.8 K (inset in Figure 6c) have been invariably interpreted[4−7] as textbook signatures of the onset of long-range ferromagnetic ordering in β-MnPc. In fact, β-MnPc is referred to in the literature as a prototypical molecular magnet.[8]

However, this established interpretation of three-dimensional (3D) long-range magnetic ordering is not supported by more detailed magnetic measurements. Figure 6b,c shows the temperature dependence of the real, χ', and imaginary, χ'', parts of the ac susceptibility of the triply sublimed pristine β-MnPc sample for several frequency values of the ac field. As it is clear, there is no anomaly in the measured ac susceptibilities at the temperature where the dc magnetization begins to increase rapidly (which we designate as T*, hereafter). If the rapid increase of the magnetization below 10 K was due to 3D long-range ordering, a divergence or critical increase of the ac susceptibility at the transition temperature should have been observed. In addition, the observed frequency dependence of the ac susceptibilities (evident at much lower temperatures than T*) also precludes true 3D ordering and implies the presence of slow relaxation of the magnetization in this temperature range. The irreversibility bifurcation in the temperature evolution of the ZFC/FC dc magnetization below 7 K as displayed in Figure 6a is also consistent with such a slow relaxation process associated with a spin freezing/blocking transition. The hysteresis loop observed during isothermal magnetization measurements at 1.8 K as shown in the inset of Figure 6c provides further evidence for freezing/blocking of the spins.

Additional strong support for the absence of 3D magnetic ordering at low temperatures also comes from heat capacity measurements (Figure 6d). The lattice contribution to the heat capacity of β-MnPc was estimated by measuring the heat capacity of isostructural β-NiPc (where Ni^{2+} is nonmagnetic) and scaling the temperature so that the data at high temperatures coincide with those of β-MnPc. Again, there is no sharp λ anomaly at around T* where a clear jump in the heat capacity should have been observed if the rapid increase in the dc magnetization was due to a true second-order phase transition with 3D coherence. Instead, there is a broad magnetic contribution distributed over a wide temperature range around 10 K, extending up to approximately 35 K. The total magnetic entropy released below 35 K is estimated from these data to be 7.9 J/mol K, which is an intermediate value between Rln2 (=5.8 J/mol K) and Rln4 (=11.5 J/mol K). Considering the absence of a λ-like anomaly in the temperature dependence of the heat capacity and the one-dimensional nature of the magnetic interaction, we can safely conclude that the observed rapid increase of magnetization below 10 K should be attributed to the increased ferromagnetic correlation length only along the molecular stacking axis (vide infra) and not to conventional three-dimensional ferromagnetic ordering as it has been universally accepted before. As the MnPc samples used for the ac susceptibility and heat capacity measurements were triply sublimed powders consisting of needlelike single crystals with macroscopic dimensions, it is unlikely that tiny amounts of residual impurities and/or lattice defects could fully suppress 3D long-range magnetic ordering.

The magnetic properties of the Li_x[MnPc] series also vary systematically upon Li doping. In Figure 7a, we show the temperature dependence of the inverse susceptibility, χ^{-1}, measured in a field of 2 kOe for selected Li_x[MnPc] compositions. All samples show a linear temperature dependence of χ^{-1}, obeying the simple Curie−Weiss expression $\chi = C/(T - \Theta)$ at least above 100 K, with the extracted Curie constants, C, and Weiss temperatures, Θ, strongly depending on the Li concentra-

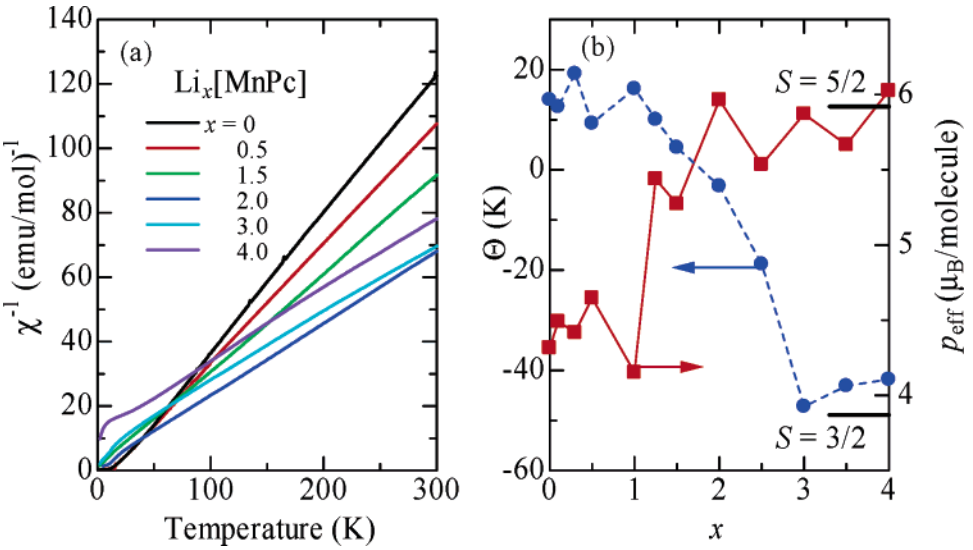

Figure 7. (a) Temperature dependence of the inverse magnetic susceptibilities, χ^{-1} (H = 2 kOe), of Li$_x$[MnPc] (x = 0, 0.5, 1.5, 2, 3, and 4). (b) Li concentration, x, dependence of the effective moment, p_{eff} (red squares), and Weiss temperature, Θ (blue circles), deduced from the Curie−Weiss fits to the inverse susceptibility data between 150 and 300 K. Horizontal bars mark the p_{eff} values that correspond to S = 3/2 and S = 5/2.

tion. Pristine β-MnPc has the smallest value of C, whereas its positive Weiss temperature, Θ, implies ferromagnetic exchange interactions and is comparable to the temperature at which the low-field magnetization begins to increase rapidly (Figure 6a). As Li is progressively intercalated in the MnPc structure, the Curie constants become larger and the Weiss temperatures shift to smaller values and change sign. The overall behavior is summarized in Figure 7b in which we show the extracted effective magnetic moment, p_{eff}, and Weiss temperature, Θ, as a function of x. When x is less than 1.25, Θ is about 10 K, and the effective moment is close to the value expected for S = 3/2 systems. In this lightly doped regime, where the intrachain interactions remain ferromagnetic, the Li$_x$[MnPc] phases display essentially identical magnetic behavior to that of the pristine material. Dc magnetization measurements also reveal the presence of irreversibility and coercivity effects below ~3 K, and the in-phase and out-of-phase ac susceptibility signals are again strongly frequency dependent, consistent with slow relaxation of the magnetization. Therefore, the one-dimensionally ordered magnetic state evidenced earlier for β-MnPc is robust against light Li doping and survives up to a doping level of $x \leq 1$. However, a drastic response of the magnetic properties is encountered when intercalation proceeds to larger values. The effective magnetic moment rapidly increases and approaches (for $x > 2$) a value corresponding to that expected for S = 5/2 systems. This is accompanied by a change in the nature of the exchange interactions which switch to antiferromagnetic as evidenced by the extracted values of Θ that become negative near $x \sim 2$ and then approach −40 K for $x > 3.0$.

Discussion

Although the intercalation chemistry of MPc with a variety of electron acceptors has been developed extensively,[14,15] at present there is no information available at all on the composition, structures, and chemical and physical properties of bulk samples of alkali-doped metallophthalocyanines, A$_x$[MPc]. Systematic studies of the effect of K doping on the conducting properties of MPc (M = Mn, Fe, Co, Ni, and Cu) thin films have revealed a rich behavior, comparable to what had been observed before in C_{60};[26] namely, the electronic properties can be controlled sensitively by the concentration of the alkali dopant and the K$_x$[MPc] films display successive insulator−metal−insulator transitions with increasing level of K doping.[23] Evidence was also presented that stable intercalated phases were formed in the K−CuPc phase field when the reaction of CuPc with potassium was carried out in the bulk.[23] Lack of single-phase samples has thus far prevented detailed structural characterization, leaving open fundamental questions such as where the alkali dopants are accommodated in the available interstitial voids and what the resultant structural modifications of the herringbone MPc structures are.

The successful synthesis of polycrystalline powders of the extended family of lithium-doped phases with composition Li$_x$[MnPc] ($0 \leq x \leq 4$) reported here has allowed us to begin to address the structural chemistry of these materials and the effect of the Li intercalation on the evolution of the electronic properties. Reaction of MnPc with lithium essentially allows quasi-continuous metal doping, affording an isostructural series of Li$_x$[MnPc] ($0 \leq x \leq 4$) solids. Despite the retention of the same monoclinic symmetry, important structural differences are apparent across the series as revealed by the results of the Rietveld refinements. In contrast to the intercalation chemistry of C_{60}, whose crystal structure contains well-defined interstitial space (tetrahedral/octahedral holes) to accommodate the alkali dopants, it is not immediately obvious how this might be achieved in the quasi-one-dimensional slipped-stacked packing architecture of the MnPc solid and raises the issue of the competition between intrachain and interchain metal incorporation with increasing doping level.

The structural results have proven sufficiently accurate to provide answers to these issues. First, for doping levels $x \leq 2$, Li^+ is exclusively accommodated within the intrastack spacing. Remarkably, the origin of the observed gradual increase in the unit cell volume (Figure 1e) is not related to a possible increase in the separation between neighboring planar MnPc molecules. Rather, the structural chemistry is driven by the strong bonding

(26) Haddon, R. C. et al. *Nature* **1991**, *350*, 320−322.

of the dopant metal ion to the pyrrole-bridging N_a atoms of the MnPc rings ($Li^+-N_a \sim 2.0$ Å, Figure 4). As a result, the slipping distance, d_2, and slipping angle, ϕ, of individual MnPc stacks increase markedly upon intercalation, and the intrastack separation, d_1, remains essentially unaffected. The increase in the slipping distance also allows Li^+ insertion without any concomitant unfavorable steric interaction with the periphery of the second neighboring MnPc molecule with which the alkali metal does not coordinate. The Li^+ defect is disordered over the two interstitial sites shown in the inset of Figure 4. As the doping level increases beyond two, these sites should become full and the inserted Li^+ should reside in additional voids. The Rietveld refinement of the diffraction data for Li_3[MnPc] reveals that, even in this case, the small size of Li^+ and its strong affinity for bonding to the ring nitrogen atoms make intrastack more energetically preferable than interstack incorporation. The Li^+ defect remains disordered over the corners of a four-membered (Li_4) ring in the space defined by adjacent planar MnPc molecules (Figure 5a) with direct coordination to four N atoms of the Pc rings. In this part of the Li−MnPc phase field, the slipping distance and angle change very little, whereas the intrastack separation begins to increase significantly for the first time. These smooth trends evident on increasing Li incorporation across the series abruptly change for the end member, Li_4[MnPc]. Here, the Rietveld refinements show that the MnPc interchain separation drastically expands as Li^+ is now also accommodated in interstitial holes between the stacks without any direct bonding interactions to the macrocycles (Figure 5b).

We now turn our attention to the discussion of the unusual magnetic properties of the Li_x[MnPc] systems, drawing from our detailed structural results. The Mn(II) ions in pristine β-MnPc are in the less-common intermediate spin ground state with $S = 3/2$ and are coupled ferromagnetically along each columnar stack. The origin of the intrachain ferromagnetic interactions has been traced to the slipped packing motif of MnPc molecules and the resultant $Mn-N_a\cdots Mn$ angle which at 93.4° is nearly optimal to allow ferromagnetic exchange interactions between the Mn d orbitals on one MnPc unit and those in neighboring units via a 90° superexchange pathway mediated by the p orbitals of the near-neighbor N_a atoms (Figure 2).[4−7] However, the magnetic data described before clearly showed that β-MnPc is not a conventional 3D ferromagnet and the observed rapid increase of the magnetization below 10 K should be attributed to the increased ferromagnetic correlation length only along the stacking axis. Actually, the magnetic properties of pristine β-MnPc are very similar to those recently reported for the α-FePc polymorph in which Fe(II) is also in the intermediate spin state with $S = 1$.[9] α-FePc also displays slow relaxation of the magnetization as evidenced by the frequency dependence of the real and imaginary parts of the ac susceptibility below about 10 K together with an irreversibility bifurcation in the dc magnetization below about 5 K and a hysteresis loop at 1.8 K. On the basis of these observations,[9] it was concluded that 3D long-range magnetic order is absent in α-FePc and a spin freezing/blocking transition occurs at about 5 K. These experimental facts are reminiscent of what we observe presently for pristine β-MnPc. In view of the similarity in the magnetic data between pristine β-MnPc and α-FePc as well as the absence of a λ-like anomaly in the heat capacity data, the low-temperature ground state of β-MnPc should therefore not be regarded as a simple 3D molecular magnet, but instead, it can be best described as comprising one-dimensional ferromagnetic segments that are strongly disordered.

The natural question that arises here is: what is the nature of the spin frozen state at low temperatures? The only possible ground states consistent with the observed phenomenology are either that of a single-chain magnet where the tunneling gaps, and hence the relaxation routes, are formed due to the Ising anisotropy of the ferromagnetically coupled spins, or that of a spin glass where the relaxation processes are determined by the local structure of the free energy. To explore this, we have displayed the frequency-dependent ac susceptibility data at fixed temperatures below the freezing/blocking temperature in the form of Cole−Cole (χ'' vs χ') plots[10−12] and have found that the resulting trajectory does not follow a semicircle curve, thereby implying that there is a distribution of relaxation times, τ, describing the behavior of the magnetization in this temperature range. This result is not in accord with the simplest case of single-chain magnets where there is a single route for the relaxation process as manifested by the semicircle trajectories of Cole−Cole diagrams of the ac susceptibilities.[10−12] Therefore, we see two possible origins of the observed distribution of relaxation times. The first is to invoke a spin glass state, which would necessitate the presence of either magnetic frustration or randomness and disorder. However, these ingredients are missing from the present material. The second possibility is that β-MnPc is a single-chain magnet, and the distribution of relaxation times arises either from the presence of multiple routes for the relaxation process even for an ideal clean sample or from the existence of a distribution of finite-length one-dimensional molecular stacks.[27] It was indeed shown recently that randomly doped magnetic chains can also display trajectories that are far from a semicircle if the collective spin reversal process of the finite-size ferromagnetically coupled spin segments works effectively.[28] Further experimental evidence such as the temperature dependence of the higher harmonics of the nonlinear susceptibility would be necessary to determine the exact nature of the ground state of pristine β-MnPc.

Next, we consider the evolution of the magnetic properties of Li_x[MnPc] with increasing Li content.[29] At low Li concentration ($x \leq 1$), there is little renormalization of the unit cell metrics and the intrachain pathway for ferromagnetic exchange interactions, described earlier for pristine β-MnPc, remains intact (Figure 2). Therefore, the materials continue to behave as 1D Ising ferromagnets with a negligible antiferromagnetic interchain exchange interaction and the observation of slow magnetic relaxation, characteristic of a spin frozen state, remains robust. However, at higher dopant concentrations ($x \geq 1.25$), the situation is drastically altered as the small electropositive Li^+

(27) We note that the details of the magnetic response of β-MnPc at low temperature are somewhat sensitive to the sample treatment (e.g., number of sublimations, sample grinding).

(28) Bogani, L.; Caneschi, A.; Fedi, M.; Gatteschi, D.; Massi, M.; Novak, M. A.; Pini, M. G.; Rettori, A.; Sessoli, R.; Vindigni, A. *Phys. Rev. Lett.* **2004**, *92*, 207204.

(29) The almost identical susceptibility data of MnPc and $Li_{1.0}$[MnPc] (Figure 7b) indicate that the doped spins do not contribute to the magnetic response. The reason for this is not presently understood. In the following, we will consider the evolution of magnetic properties of the Li_x[MnPc] series as that of the Mn d spins.

does not behave as an innocent spacer residing in the available void space without interacting with the host molecules. As a result, the increased dopant level has important structural and electronic consequences leading to (i) an increased slippage (d_2) of adjacent MnPc units and (ii) a strong coordination of Li^+ to the pyrrole-bridging N_a atoms of the macrocycles. In the following, we consider these points in more detail.

First, the increased slippage of adjacent MnPc molecules leads to an opening up of the Mn−N_a···Mn angles. According to the structural results, the values increase from 93.4° for pristine MnPc to 98.1° and 98.4° for Li_x[MnPc] with $x = 1.5$ and 3, respectively, and then decrease to 95.1° for $x = 4$. As a Mn−N_a···Mn angle of 90° is optimal for ferromagnetic intrachain interaction, the pristine sample has the strongest tendency to display ferromagnetic interactions along the stacks. As the Li intercalation proceeds beyond 1 and the angle becomes larger, the exchange interactions switch from ferromagnetic to antiferromagnetic. Such a delicate competition between exchange interactions with opposite signs as a function of bond angle has been also theoretically predicted[30] for edge-sharing Cu−O chain systems, with the sign change of the interaction having been reported to occur at an angle between 95° and 99.1°.

Second, the intercalated Li^+ ions strongly coordinate to the same pyrrole-bridging N_a atoms of the macrocycle, implicated in the ferromagnetic Mn−N_a···Mn superexchange pathway, thereby competing effectively for the available electron density and strongly modifying the electronic structure. In MnPc, each Mn^{2+} ion is coordinated to four equatorial nitrogen atoms of the same molecule and two apical N_a atoms from adjacent molecules at a longer distance (Figure 2). Given the short Li^+−N_a bond length in Li_x[MnPc], the charge density distribution of the donated electron by Li is not delocalized over the whole macrocyclic skeleton but should reside exclusively on the N_a atoms with no interaction with the Mn(II) ions whose oxidation state does not change in the course of Li intercalation. In such a case, the ligand field that is produced by the four equatorial nitrogen atoms remains essentially unchanged, and the Coulomb potential produced by the apical N_a atoms becomes stronger. As a result, the local environment of the Mn^{2+} ion and the modified ligand field resemble those of a field with cubic symmetry, where the high-spin (low-spin) state is favored over the intermediate spin state if the splitting between the t_{2g} and e_g levels is small (large). According to molecular orbital calculations,[31] the electron density at the equatorial N atoms is relatively small, implying that the ligand field splitting is also small. The resultant renormalization of the energies of the d orbitals would be responsible for the observed spin-state transition of Mn^{2+} from the intermediate spin, $S = 3/2$, to the high spin, $S = 5/2$, state.

Finally, we discuss the effect of the structural evolution upon Li intercalation on the conducting properties. Despite the charge injection into the MnPc molecules, the resistivity has not shown a drastic decrease upon the Li intercalation (Supporting Information Figure 1S). We attribute the robust insulating behavior principally to the survival of the slipped stacking architecture with poor $\pi-\pi$ overlap of the electron wave functions along the chain direction, as revealed by the Rietveld refinements of the structure. We also note that in hole-doped MPc solids[14,15] metallic behavior has been encountered only when the slippage is eliminated ($d_2 = 0$) and the molecules stack cofacially with a twist angle in the vicinity of 45°. In addition, the intercalated Li^+ ions in Li_x[MnPc] are strongly bound to pyrrole-bridging N_a atoms in the intrastack spacing, thereby perturbing strongly the electronic structure and reducing further the intrastack electron-transfer integral. Because of the formation of Li^+−N_a bonding, donated electrons from the metal atoms are strongly localized on the N_a atoms. These combined effects seem to preclude electrical conduction along the chain direction in the present system. The experimental situation also appears different from the effect of K doping on the evolution of the transport properties in thin-film samples[23] of MPc where metallic behavior is observed for certain doping levels. Though there is no detailed characterization of the structural evolution on doping, MPc thin films typically adopt the α-type polymorphic form of molecular stacking in which the slippage angle along the chain direction is significantly reduced to ∼25°. Assuming that this molecular stacking motif is retained for the K_x[MPc] thin films and that the larger more electropositive K^+ ions occupy off-chain interstices, the $\pi-\pi$ overlap integral could be larger thereby leading to the observed increased conduction.

Conclusions

We have discovered that the magnetic ground state of β-MnPc, in which the Mn^{2+} ion adopts the unusual intermediate spin state with $S = 3/2$, can be best described as ferromagnetically ordered chains that are disordered in three dimensions in contrast to the established view of a classical three-dimensionally ordered molecular magnet. We have also successfully synthesized the first example of a series of alkali-metal-doped MPc phases, Li_x[MnPc] ($0 \le x \le 4$), and clarified the evolution of their structural and magnetic properties with increasing doping level, x. Inserted Li^+ ions strongly bond to pyrrole-bridging nitrogen atoms of the Pc rings and drive the structural change when the doping level x exceeds 1. The intrachain exchange interaction has been found to change from ferromagnetic to antiferromagnetic as the Li concentration is increased, and at the same time, the spin state changes from intermediate (IS, $S = 3/2$) to high spin (HS, $S = 5/2$). We have described how the details of the structural changes are relevant in the understanding of the observed variation in the magnetic properties. The present work opens the way for the isolation and study of new families of molecule-based charge-transfer systems, A_x[MPc] (where A denotes alkali metal), with low-dimensional electronic structures and strong electron correlations in which the MPc units act as electron acceptors. Given the wealth of intriguing phenomena predicted theoretically for these systems,[24] it would be very interesting to explore experimentally the structural and electronic consequences of varying the size and electropositive character of the alkali dopant, A, as well as the nature and electronic configuration of the central metal ion, M(II).

Acknowledgment. We acknowledge K. Osaka, M. Takata, and M. Brunelli for help with the experiments and M. F. Craciun

(30) Mizuno, Y.; Tohyama, T.; Maekawa, S.; Osafune, T.; Motoyama, N.; Eisaki, H.; Uchida, S. *Phys. Rev. B* **1998**, *57*, 5326−5335.
(31) Liao, M.-S.; Scheiner, S. *J. Chem. Phys.* **2001**, *114*, 9780−9791.

and A. F. Morpurgo for enlightening discussions. We thank SPring-8 and the ESRF for synchrotron X-ray beamtime. This work was supported by a Grant-in-Aid for Scientific Research from MEXT, Japan, by the Royal Society (Dorothy Hodgkin Research Fellowship to S.M.) and by the Daiwa Anglo-Japanese Foundation.

Supporting Information Available: Tables of the refinement parameters, figure of the Li-doping dependence of the ambient-temperature resistivity, and full list of authors of ref 26. This material is available free of charge via the Internet at http://pubs.acs.org.

JA0582657